HHS Public Access

Author manuscript

Mol Imaging. Author manuscript; available in PMC 2017 August 07.

Published in final edited form as:

Mol Imaging. 2014 ; 13: .

Imaging Dopaminergic Dysfunction as a Surrogate Marker of Neuropathology in a Small Animal Model of HIV

Dianne E. Lee[1], **William C. Reid**[1], **Wael G. Ibrahim**[1], **Kristin L. Peterson**[1], **Margaret R. Lentz**[1], **Dragan Maric**[2], **Peter L. Choyke**[3], **Elaine M. Jagoda**[3], and **Dima A. Hammoud**[1,*]

[1]Center for Infectious Disease Imaging (CIDI), Radiology and Imaging Sciences, National Institutes of Health, Bethesda, Maryland, USA

[2]Division of Intermural Research (DIR), National Institute of Neurological Disorders and Stroke (NINDS), National Institutes of Health, Bethesda, Maryland, USA

[3]Molecular Imaging Program (MIP), National Cancer Institute (NCI), Bethesda, Maryland, USA

Abstract

The dopaminergic system is especially vulnerable to the effects of HIV infection rendering dopaminergic deficits early surrogate markers of HIV-associated neuropathology. We quantified dopamine $D_{2/3}$ receptors in young HIV-1 transgenic (Tg) (n=6) and age-matched control rats (n=7) and adult Tg (n=5) and age-matched control rats (n=5) using [^{18}F]fallypride PET. Regional uptake was quantified as binding potential (BP_{ND}) using the two-tissue reference model with cerebellum as reference. Time activity curves were generated for the ventral striatum (VS), dorsal striatum (DS), thalamus (Th), and cerebellum. While BP_{ND} values were significantly lower in the VS (p<0.001) and DS (p=0.001) in the adult Tg rats compared to controls rats, they were significantly lower only in the DS (p<0.05) in the young rats. Tg rats had smaller striatal volumes on MRI. We also found lower expression levels of tyrosine hydroxylase on immunohistochemistry in the Tg animals. Our findings suggest that progressive striatal $D_{2/3}$ receptor deficits occur in Tg rats as they age and can be detected using small animal PET imaging. Effectiveness of various approaches in preventing/halting this dopaminergic loss in the Tg rat can thus be measured preclinically using [^{18}F]fallypride PET as a molecular imaging biomarker of HIV-associated neuropathology.

Keywords

HIV; neuro-HIV; transgenic rat; [^{18}F]fallypride; dopamine $D_{2/3}$ receptors; PET

1. Introduction

One of the well-acknowledged goals of molecular imaging is the development of reliable, reproducible and sensitive non-invasive imaging biomarkers of disease that can assist in the evaluation of novel therapies at the preclinical and translational levels. Many disciplines in

*Corresponding author: Dima A. Hammoud, MD, National Institutes of Health/Clinical Center, 10 Center Drive, Room 1C368, Bethesda, MD 20814-9692, Phone: 301-402-3041, Fax: 301-496-9933, hammoudd@cc.nih.gov.

medicine are in dire need for such biomarkers, and the field of neuro-HIV is no exception. This is especially true considering the escalating problem of HIV-associated neurocognitive disorders (HAND) with about 52% of HIV-positive (HIV+) individuals currently thought to be affected, despite optimal antiretroviral therapy and peripheral control of the infection [1]. Developing neuro-protective therapies for those patients is of utmost importance, and towards that goal, reliable reproducible biomarkers of brain damage need to be developed and validated.

Neuro-HIV research is however hampered by two major issues: the lack of validated small animal model (mice and rats are non-permissive for HIV infection [2]) and the lack of objective measurable biomarkers of disease. Short of using expensive and sentient SIV infected monkeys, the HIV-1 transgenic (Tg) rat is considered a good model of HIV. This rat model expresses 7 of the 9 HIV-1 viral proteins including gp120, nef, and Tat but most importantly is known to develop clinically relevant neuropathologies [3] and cognitive deficits [4–7]. Interestingly, dopaminergic system dysfunction in this animal model has been demonstrated repeatedly [4, 8, 9]. This is not unusual considering the known vulnerability of the dopaminergic system to the effect of the virus, with the latter selectively targeting the basal ganglia [10] and resulting in well recognized parkinsonian-like symptomatology in infected patients [11–14].

In this report, we evaluated the dopaminergic system in the Tg rat using *in vivo* positron emission tomography (PET) imaging and [^{18}F]fallypride, a fluorinated Dopamine $D_{2/3}$ receptor high affinity antagonist (K_D=33 pmol/l). We hypothesized that alterations in striatal $D_{2/3}$ receptors will be detected by [^{18}F]fallypride PET imaging in the Tg rats compared to controls and that [^{18}F]fallypride PET can be used as a biomarker for neuropathology in the Tg rat. We also performed high-field MR imaging in the Tg and control rats in order to correlate structural volumetric changes with changes in striatal $D_{2/3}$ receptor density. Finally, we correlated the structural and PET findings with immunofluorescent staining of brain striatal slices from Tg and control animals at different ages.

2. Material and methods

2.1. [^{18}F]fallypride PET scanning

2.1.1 Animals—The young animal group consisted of 6 male Tg (3.0 ± 0.4 months; 265 ± 29 g) and 7 male age-matched Fisher F344 control rats (3.0 ± 0.2 months; 283 ± 26 g). The older animal group consisted of 5 adult male HIV-1 Tg (15.2 ± 0.4 months; 380 ± 28 g) and 5 adult male control rats (15.6 ± 0.4 months; 486 ± 46 g). All the animals were obtained from Harlan Inc. (Indianapolis, IN). All rats were housed in a temperate-controlled environment with a 12 h light/dark cycle. The animals were allowed free access to food and water. All procedures were conducted during the light cycle. Rats were carefully handled for 3 days prior to various experiments to minimize handling-related stress. Animal care and all experimental procedures were approved by the Animal Care and Use Committee of the National Institutes of Health.

2.1.2. Radioligand Preparation—The radiosynthesis of [^{18}F]fallypride was performed according to the protocol of Mukherjee et al. [15]. The chemical purity was consistently

found to be > 99 % with specific radioactivities ranging between 1.4 and 3.3 Ci/μmol (52 and 121 GBq/μmol) and activity concentrations ranging between 1.79 to 3.79 mCi/ml (66 to 140 MBq/ml).

2.1.3. PET Scanning—Two rodents were scanned per day and the order of scanning was strictly counterbalanced: one Tg rat and one control rat, in alternative order. Animals were anesthetized with 2–2.5 % isoflurane air/oxygen mixture. The intra-subject variability of the depth of anesthesia was monitored by measuring respiratory frequency periodically during the scan. PET experiments were performed on a Bio PET/CT tomograph (Bioscan Inc., Washington, D.C.) with an axial field of view (FOV) of 4.8 cm and 6.7 cm in diameter. Time coincidence window was set to 10 ns with an energy window of 250–700 keV. The lateral tail vein was cannulated for injection of radiotracer, and the cannula was then connected to a heparin lock and secured in place with medical tape. The animal was positioned prone with the head placed symmetrically in the center field of view (FOV) on the thermostatically heated bed supplied by the manufacturer (Bioscan Inc., Washington, D.C.). [^{18}F]fallypride injection of 1.06 ± 0.18 mCi (39.2 ± 6.7 MBq; 1.97 ± 1.05 nmol/kg body weight) was then administered as a slow bolus injection (over 30s) into the indwelling intravenous catheter followed by a 300 μl saline flush (maximum volume of injection= 600 μl). PET emission data was acquired for 90 minutes in list mode. The resultant emission sinograms for each frame were then corrected for scatter, ^{18}F decay, randoms, and deadtime. The datasets were reconstructed into a dynamic sequence of 14 individual frames (6 × 60 s, 1 × 300 s, 7 × 600 s) using FORE and ordered subject expectation maximization (OSEM-2D; 16 subsets and 4 iterations) algorithm with a bin size of 0.39 mm, a matrix size of 175 × 175 × 61, and resolution recovery of 2.1 mm FWHM.

2.2. Magnetic Resonance Imaging (MRI)

Imaging was performed on a 7T Bruker Biospin system (Billerica, MA) using a rapid acquisition with refocused echo (RARE) sequence with animals under 1.5 % isoflurane anesthesia. The animals were placed in an imaging cradle that allowed for stereotactic alignment of the head. Each animal was monitored by respiration and body temperature over the course of the experiments. A cross coil setup was used which included a 20 mm surface coil placed on the head of the animal while transmission was performed using a 72 mm transmit coil. A series of sagittal T2-weighted MR images were initially obtained, in the center of the brain to allow for consistent positioning of the coronal T2- weighted images with respect to the genu of the corpus callosum. Parameters included echo time (TE) of 49.18 ms, repetition time (TR) of 1000 ms, 0.14 × 0.14 mm/pixel spatial resolution, 256 × 256 matrix size, 8 averages, RARE factor of 8, FOV of 35 × 35 mm, and sagittal (five) 0.5 mm thick slices. Coronal T2-weighted MR images were acquired to allow for co-registration with PET images and volume analysis. Parameters included TE of 12.3 ms, TR of 3379 ms, 0.14 × 0.14 mm/pixel spatial resolution, 256 × 256 matrix size, 8 averages, a RARE factor of 8, FOV of 35 × 35 mm, and coronal 1 mm slice thickness. The NIH open source software, medical image processing, analysis and visualization (MIPAV) was used for the manual masking, volume of interest (VOI) placement, and volume calculations of the whole brain (WBV) and of the striatum. Striatal volume (SV) measurements were based on three slices

from the coronal T2 experiment, positioned at approximately Bregma −0.6 through 1.44 determined by comparing the co-registered T2 images to the Paxinos rat brain atlas [16].

2.3. Dynamic Modeling of Volumes of Interest (VOIs) on PET and MRI

The reconstructed PET images were spatially normalized into a standard space using an MRI atlas provided by Schweinhardt et al. [17] which is in stereotaxic space using a rigid body transformation matrix. VOIs were drawn over the relevant regions (ventral striatum (VS), dorsal striatum (DS), thalamus (Th), and cerebellum) using the co-registered MRI for guidance [17] and an anatomical atlas of the rodent brain [16]. The rat striatum was clearly visible bilaterally and delineated as previously described [18]. Separate VOIs were drawn in the left and right hemispheres and the values were then averaged. To minimize partial volume effects, VOIs were placed centrally within the structures. Time-activity curves (TACs) were generated for the VOIs. Image analyses were performed using PMOD 3.4 kinetic modeling tool (PMOD Technologies Ltd., Zurich, Switzerland). The cerebellum served as a reference tissue for receptor quantification due to its low D_2 receptor density [19]. To derive estimates for binding potential (BP_{ND}) of [^{18}F]fallypride, TACs were fit to Watabe's reference tissue model with two compartments [20], an extension of the simplified reference model [21]. This new reference tissue model assumes that the reference region can be expressed as two-tissue compartments instead of the more conventional single-tissue compartment. Thus, the BP_{ND} can be estimated as follows assuming that the nonspecific binding is uniform across the tissues [22]:

$$C(t)=R_1[C'(t)+\mathrm{aC}'(t)\otimes e^{-(k_3'+k_4')t}+\mathrm{bC}'(t)x\otimes e^{-k_2 t}]$$

$$a=\frac{k_3'k_2'}{k_3'+k_4'-k_2}$$

$$a=\frac{k_2^2-k_2(k_2'+k_3'+k_4')+(k_2'k_4')}{k_3'+k_4'-k_2+}$$

$$\mathrm{BP}_{\mathrm{ND}}=\frac{K_1k_2'}{K_1'k_2\left(1+\frac{k_3'}{k_4'}\right)}-1$$

R_1 corresponds to the differences in uptake between specific and reference regions (R_1 = K_1/K_1'). Parameters K_1 (ml/min/min), k_2, and k_2' are rate constants (min^{-1}) for transfers across the blood-brain barrier (BBB). Parameters k_3 (min^{-1}) and k_4' (min^{-1}) are rate constants for transfers between non-displaceable and specifically bound compartments. When the parameters k_2', k_3', and k_4' are fixed to constants determined with receptor-rich tissue, only R_1 and k_2 need to be fitted for estimating the BP_{ND}.

In one control rat, test-retest variability of [^{18}F]fallypride between scan days 1 and 2 (less than 2 weeks apart) was evaluated.

2.4. Immunofluorescence

Rat brain sections at the level of the striatum were evaluated and compared in nine young (3-month-old) animals (5 Tg and 4 controls), seven adult (7 to 9-month-old) animals (5 Tg and 3 controls) and three older (15-month-old) animals (2 Tg and 1 control).

Preparation of brain tissues for staining—Rats were first anesthetized with Isoflurane (3% with 700cc/min O2). This was followed by transcardial perfusion using 100 ml of normal saline (pH=7.4) and 350 ml of freshly prepared and filtered (0.45 micron filter) 4% paraformaldehyde (pH 7.4). Brains were removed and post-fixed overnight in 4% paraformaldehyde at 4°C followed by three one-hour washes in normal saline at 4°C. Brains were next cryoprotected in 10% sucrose and stored at 4°C until they sank in the solution; they were subsequently placed in 20% and then 30% sucrose until they sank again in each solution. The brains were then embedded in optimal cutting temperature compound (O.C.T., Tissue-Tek ®) and ten-micron thick coronal serial sections were obtained. The striatal sections (Bregma 0.48 mm to 0.12 mm) were then selected for immunofluorescent staining.

Multiepitope immunolabeling protocols were applied to the prepared fresh frozen striatal brain slices to identify the cellular phenotypes using different combinations of primary antibodies that included guinea pig IgG anti-NeuN (EMD Millipore, cat# ABN90P) to identify most neurons, chicken IgY anti-tyrosine hydroxylase (TH) (Abcam, cat# ab76442) to identify dopaminergic neurons and mouse IgG2b anti-GFAP (BD Biosciences, cat# 556330) to identify astrocytes. Each of the above primary immunoreactions was visualized using appropriate fluorophore-conjugated (Alexa Fluor dyes) secondary antibodies obtained either from Jackson ImmunoResearch or Life Technologies/Invitrogen. The cell nuclei were counterstained using 1 ug/ml of 4',6-diamidino-2-phenylindole (DAPI) to facilitate cell counting. All fluorescence signals were imaged using an Axio Imager.Z2 upright scanning wide field fluorescence microscope (Zeiss) equipped with Orca Flash 4.0 high resolution sCMOS camera (Hamamatsu), 200W X-cite 200DC broadband light source (Lumen Dynamics) and standard DAPI, and respective Alexa Fluor filter sets (Semrock). After imaging, the multichannel image datasets were processed for image stitching, illumination correction and then were imported into Adobe Photoshop CS6 to produce pseudo-colored multi-channel composites.

2.5. Statistical Analyses

The results are represented as mean ± standard deviation (M ± s.d.). The differences in the BP_{ND} estimates were compared for the two groups using two-sample Student's *t*-tests and were considered significant at *P*-value <0.05. Test-retest variability of [^{18}F]fallypride uptake in brain regions between days 1 and 2 was calculated as : $[BP_{day1} - BP_{day2}]/[BP_{day1+}BP_{day2}]/2 \times 100$.

3. RESULTS

3.1. [^{18}F]fallypride PET scanning

3.1.1. Animal group comparisons—Body weight was recorded prior to each imaging session. The 3 month-old Tg (265 ± 30 g) and control (283 ± 30 g) groups did not significantly differ in their body weight (p=0.25), but the 16 month-old Tg rats (380 ± 30 g) weighed significantly less than the age-matched controls (486 ± 50 g; p<0.001).

3.1.2. [^{18}F]fallypride injection characteristics—In the young cohort, the Tg rats did not differ from controls with regard to injected dose (1.03 ± 0.25 vs. 0.83 ± 0.26 mCi; p=0.20) (38 vs. 31 MBq), [^{18}F]fallypride specific activity (1.35 ± 0.55 vs. 0.94 ± 0.31 Ci/μmol; p=0.10) (50 vs. 35 GBq/μmol) or injected mass per body weight (3.18 ± 1.06 vs. 3.02 ± 0.64 nmol/kg; p=0.75).

Similarly, in the adult cohorts, no statistically significant differences were observed in injected dose [Tg: 1.03 ± 0.29 mCi (38 MBq); control: 1.10 ± 0.40 mCi (41 MBq); p=0.76], [^{18}F]fallypride specific activity [Tg: 1.94 ± 0.69 Ci/μmol (72 GBq/μmol); control: 1.69 ± 0.40 Ci/μmol (63 GBq/ μmol); p=0.51] or injected mass even when normalized for the body weight (Tg: 1.45 ± 0.16 nmol/kg; control: 1.33 ± 0.22 nmol/kg; p=0.36).

In the animal which underwent test and retest scans, there were no differences between scan 1 (test) and scan 2 (retest) in injected dose, specific radioactivity or injected mass even when normalized for the animal's weight.

3.1.3. [^{18}F]fallypride Images—Injection of approximately 1 mCi of [^{18}F]fallypride using the Bio PET/CT tomograph resulted in high-resolution images of the rat striatum and high signal to noise ratios. Lower activity concentrations were seen in the thalamus, an extrastriatal region. Regional distribution of [^{18}F]fallypride in a representative adult Tg (Figure. 1A) and adult control rat (Figure. 1B) are shown.

3.1.4. Time-Activity Curves (TACs)—Figure 1 also depicts the typical [^{18}F]fallypride TACs for an adult Tg (1C) and age-matched adult control rat (1D), calibrated to unit nCi/mL. Data is shown for the DS, VS, Th and cerebellum over the total scan duration of 90 minutes. An example of the quality of the data fit obtained using Watabe's reference tissue model with two compartments [20] is shown as solid lines (Figures. 1C and 1D). As expected, the highest uptake of [^{18}F]fallypride was seen in the striatal regions with moderate uptake in the thalamus, and low uptake in the cerebellum. These results are consistent with the known distribution of $D_{2/3}$ receptors in humans [23].

3.1.5. $D_{2/3}$ receptor availability—Region of interest comparisons showed a statistically significant reduction of BP_{ND} in the DS for young (14%; p<0.05) and adult (33%; p<0.001) Tg rats relative to age-matched control rats (Fig. 3). BP_{ND} estimates in the VS for the adult Tg group showed significant reduction compared to age-matched controls (36%; p<0.001). In the young group, although the Tg rats tended to have lower BP_{ND} values in the VS (14%) relative to controls, this was not statistically significant (p=0.11). No statistically significant

BP_{ND} differences were observed in the thalamus, neither in the young nor in the old group (Figure. 2).

Percentage test-retest differences of [^{18}F]fallypride BP_{ND} were highly reproducible. Less than 7.6 % variability was observed in the striatal VOIs.

3.2. Magnetic resonance imaging results

Upon reviewing the MR images, we noted that many Tg animals showed increased ventricular size over time, while the control animals did not. The representative SV values measured on MRI were smaller in the young Tg (73 ± 3.04 μl) compared to the young controls (74.56 ± 2.85 μl) however this was not statistically significant (p=0.44). In the older animal group, on the other hand, SVs in the Tg animals were significantly smaller (8%) than the control animals (71.23 ± 1.77 versus 76.69 ± 3.56 μl, p<0.05) (Figure. 3A). For the WBV, decreased values were seen in the Tg rats compared to age-matched controls (young and adults). Those reductions however were not statistically significant (Figure. 3B).

3.3. Immunofluorescence

Immunofluorescent staining for TH showed decreased staining in the striatum of Tg animals compared to age-matched controls in all three groups. Examples from the three age groups are shown in Figure. 4. Those changes were least noticeable in the young animal group (3-month-old, panel 4A). In general, the staining appeared diffusely decreased in the Tg rats in comparison to age-matched controls in one out of three young, one out of three adult and one out of two older Tg animals, while it appeared more focally decreased in the rest of the Tg animals compared to their age-matched controls. The focal decreased staining pattern is depicted in Figure 4, panel C, while the diffuse decreased staining pattern is better appreciated in panel 4B. Other findings included astrocytic dysfunction seen as abnormally decreased GFAP staining, as well as decreased striatal Neu-N staining, a marker of neuronal integrity (data not shown).

4. Discussion

With their non-acute onset and relatively subtle initial clinical presentations, the mild forms of HAND lead to gradual, but ultimately significant functional deterioration that often complicates the management of HIV+ patients and affect their quality of life [1]. Those conditions persist nowadays despite successful suppression of the virus in the periphery. One neurotransmitter system that seems to be especially vulnerable to the effects of the virus is the dopaminergic system [10]. Involvement of the dopaminergic system in neuro-HIV explains the previously described Parkinsonian-like symptomatology in the setting of HIV infection [11–14], and also explains findings of lower dopamine transporter levels in the putamina of HIV+ subjects when compared to healthy controls (HIV: −12.2%, p = 0.02), as detected by PET [24].

In our study, we wanted to validate an appropriate animal model of neuro-HIV and dopaminergic dysfunction along with a non-invasive *in vivo* imaging biomarker, so that the combination can then be used for preclinical evaluation of neuroprotective therapies and their potential at halting or preventing brain damage. As a small animal model, we used the

HIV-1 Tg rat, a non-infectious model of HIV infection, in which the expression of the transgene, consisting of an HIV-1 provirus with functional deletion of gag and pol, is regulated by the viral long terminal repeat [3]. There is no potential for replication, but there is chronic exposure to viral proteins. We chose the Tg rat as it has been found consistently to exhibit pathologies and immune irregularities characteristic of HIV-1 infection of humans including neurological signs and behavioral abnormalities [3–5, 8, 9, 25].

Using PET imaging with [18]fallypride, a high affinity Dopamine $D_{2/3}$ receptor antagonist, we found significantly decreased $D_{2/3}$ receptors in the adult Tg rat brains compared to age-matched controls, both in the DS and VS (Figure. 2). In younger animals the decrease was only significant in the DS (Figure. 2), which suggests a continuous trend of neurological/dopaminergic damage that worsens with age. We corroborated our findings with structural MR imaging of the same animals used for PET imaging, where we detected decreased striatal volumes in the Tg rats compared to controls. Interestingly, the decreased SV was statistically significant in the older but not in the younger Tg rats (Figure. 3A), while the WBV values were not significantly different at either age (Figure. 3B). We concluded that the striatum in the Tg brain must be undergoing an accelerated rate of atrophy with aging that is out of proportion to the total brain volume loss, a phenomenon that is not seen in control animals, where the rate of SV loss seemed to be proportional to that of the total brain volume loss (Figure. 3B). The findings are also consistent with our observation of increased ventricular volume in the older but not in the younger Tg rats, probably due to atrophy of the adjacent striatum.

Furthermore, immunofluorescent staining of Tg and control brains showed decreased (either diffuse or focal) TH staining in the striatum of Tg rats compared to age-matched controls at all ages (Figure. 4). Those findings were however less prominent in the 3-month-old animals. The combination of decreased TH (early step in dopamine synthesis) and decreased post synaptic receptor density ($D_{2/3}$) supports the notion of dopaminergic neuronal dysfunction/loss in this animal.

The exact neuropathology leading to HAND is not yet fully understood. Unlike microglia, neurons do not express CD4 and although there are a few reports of presence of HIV proviral DNA in neurons [26, 27], there still is no direct evidence of productively infected neurons with HIV [28, 29]. The neurologic damage is rather thought to be related to persistent low level neuroinflammation [30, 31], neurotoxic effects of viral proteins [32, 33], as well as the indirect disruption of the supportive and neurotrophic role of astrocytes [34] and oligodendrocytes [35].

In our animal model, we believe the damage to be mainly related to chronic exposure of various brain cells to viral proteins, such as gp120, Tat and nef, which we have shown to be produced locally in the Tg rat brain and present at high concentrations in the CSF (unpublished data). HIV-1 viral proteins are in fact known to cause neuronal damage [36–39] with at least one of them, Tat, causing reduced evoked dopamine release and dysfunction in dopamine terminal field [40].

Irrespective of the exact mechanism of neurotoxicity, we have shown that [^{18}F]fallypride can detect dopaminergic system dysfunction in the Tg rats and potentially can be used as a biomarker of disease severity/neurodegeneration in this non-infectious animal model of HIV. This ligand, [^{18}F]fallypride, a fluorinated $D_{2/3}$ high affinity antagonist (K_D=33 pmol/l), is perhaps one of the best characterized $D_{2/3}$ radioligands, and has been used extensively in clinical studies of psychiatric disease [41–43]. It localizes selectively to the $D_{2/3}$ receptors, both in the striatal and extrastriatal brain regions of rodents [18, 44–46], humans [47, 48] and non-human primates [49]. It is available in many large PET centers, and has multiple advantages over similar ligands, such as the ability to image receptors in low concentrations (<1 nmol/l) and to image extrastriatal D_2/D_3 receptors with sufficient target-to-background signal to detect subtle changes in the specific binding in those regions.

Our study is slightly limited by lack of longitudinal data in the same animals and lack of imaging in middle-aged animals (9–11 months). Both limitations are being addressed in the second phase of the study. Our volume data is also limited by the difficulty of delineating the exact anterior and posterior borders of the striatum on the coronal MR images. We believe however that we have captured the majority of the caudate and putamen, in the same exact location, in every animal. Another issue is the use of anesthesia, which is generally required for small animal imaging. Tantawy and colleagues [50] reported 13.7% lower striatal [^{18}F]fallypride BP_{ND} estimates with 1.5 % isoflurane-anesthetized rats vs. conscious uptake of the radiotracer. In our work, the animal preparation for imaging and the anesthetic agent administered (isoflurane 2–2.5 %) were identical between all imaged animals. In fact, our experimental conditions on two different days in the test-retest resulted in a < 7.6 % change in BP_{ND} in the striatal regions. Otherwise, we are not aware of blood metabolite changes of [^{18}F]fallypride due to isoflurane.

In conclusion, our ultimate goal was to identify a quantifiable dopaminergic dysfunction biomarker that can be used to test the potential of HIV neuroprotective therapies in a suitable small animal model. We found that the HIV-1 Tg rat is a good model for dopaminergic dysfunction in HIV. Various approaches/therapies for preventing this dopaminergic loss, which can be measured using [^{18}F]fallypride PET, could eventually prove useful in preventing/halting neurocognitive dysfunction in HIV+ patients.

Acknowledgments

This work was supported by the Center of Infectious Disease Imaging (CIDI), National Institutes of Health (Intramural Program).

Abbreviations

BP_{ND}	Binding potential
DS	Dorsal striatum
TE	Echo time
FOV	Field of view
Tg	HIV-1 transgenic

HAND	HIV-associated neurocognitive disorders
IHC	Immunohistochemistry
RARE	Rapid acquisition with refocused echo
ROI	Region of interest
TR	Repetition time
SV	Striatal volume
Th	Thalamus
TAC	Time-activity curve
TH	Tyrosine Hydroxylase
VS	Ventral striatum
VOI	Volumes of interest
WBV	Whole brain volume

References

1. Heaton RK, et al. HIV-associated neurocognitive disorders persist in the era of potent antiretroviral therapy: CHARTER Study. Neurology. 2010; 75(23):2087–96. [PubMed: 21135382]
2. Bieniasz PD, Cullen BR. Multiple blocks to human immunodeficiency virus type 1 replication in rodent cells. J Virol. 2000; 74(21):9868–77. [PubMed: 11024113]
3. Reid W, et al. An HIV-1 transgenic rat that develops HIV-related pathology and immunologic dysfunction. Proc Natl Acad Sci U S A. 2001; 98(16):9271–6. [PubMed: 11481487]
4. Moran LM, et al. Adolescent HIV-1 transgenic rats: evidence for dopaminergic alterations in behavior and neurochemistry revealed by methamphetamine challenge. Curr HIV Res. 2012; 10(5): 415–24. [PubMed: 22591365]
5. Moran LM, Booze RM, Mactutus CF. Time and time again: temporal processing demands implicate perceptual and gating deficits in the HIV-1 transgenic rat. J Neuroimmune Pharmacol. 2013; 8(4): 988–97. [PubMed: 23690140]
6. Lashomb AL, Vigorito M, Chang SL. Further characterization of the spatial learning deficit in the human immunodeficiency virus-1 transgenic rat. J Neurovirol. 2009; 15(1):14–24. [PubMed: 19085205]
7. Peng J, et al. The HIV-1 transgenic rat as a model for HIV-1 infected individuals on HAART. J Neuroimmunol. 2010; 218(1–2):94–101. [PubMed: 19913921]
8. Moran LM, et al. Neurobehavioral alterations in HIV-1 transgenic rats: evidence for dopaminergic dysfunction. Experimental neurology. 2013; 239:139–47. [PubMed: 23063600]
9. Webb KM, et al. Evidence for developmental dopaminergic alterations in the human immunodeficiency virus-1 transgenic rat. J Neurovirol. 2010; 16(2):168–73. [PubMed: 20337512]
10. Nath A, et al. Neurotoxicity and dysfunction of dopaminergic systems associated with AIDS dementia. Journal of psychopharmacology. 2000; 14(3):222–7. [PubMed: 11106300]
11. Hersh BP, Rajendran PR, Battinelli D. Parkinsonism as the presenting manifestation of HIV infection: improvement on HAART. Neurology. 2001; 56(2):278–9. [PubMed: 11160977]
12. Koutsilieri E, ter Meulen V, Riederer P. Neurotransmission in HIV associated dementia: a short review. J Neural Transm. 2001; 108(6):767–75. [PubMed: 11478426]
13. Lopez OL, et al. Dopamine systems in human immunodeficiency virus-associated dementia. Neuropsychiatry Neuropsychol Behav Neurol. 1999; 12(3):184–92. [PubMed: 10456803]

14. Mirsattari SM, Power C, Nath A. Parkinsonism with HIV infection. Mov Disord. 1998; 13(4):684–9. [PubMed: 9686775]
15. Mukherjee J, et al. Measurement of d-amphetamine-induced effects on the binding of dopamine D-2/D-3 receptor radioligand, 18F-fallypride in extrastriatal brain regions in non-human primates using PET. Brain research. 2005; 1032(1–2):77–84. [PubMed: 15680944]
16. Paxinos, G., Watson, C. The Rat Brain: In Stereotaxic Coordinates. Academic Press; 1998. p. 237Incorporated, 1998
17. Schweinhardt P, et al. A template for spatial normalisation of MR images of the rat brain. J Neurosci Methods. 2003; 129(2):105–13. [PubMed: 14511814]
18. Dalley JW, et al. Nucleus accumbens D2/3 receptors predict trait impulsivity and cocaine reinforcement. Science. 2007; 315(5816):1267–70. [PubMed: 17332411]
19. Farde L, et al. Quantitative analysis of D2 dopamine receptor binding in the living human brain by PET. Science. 1986; 231(4735):258–61. [PubMed: 2867601]
20. Watabe H, et al. Kinetic analysis of the 5-HT2A ligand [11C]MDL 100,907. Journal of cerebral blood flow and metabolism : official journal of the International Society of Cerebral Blood Flow and Metabolism. 2000; 20(6):899–909.
21. Lammertsma AA, Hume SP. Simplified reference tissue model for PET receptor studies. Neuroimage. 1996; 4(3 Pt 1):153–8. [PubMed: 9345505]
22. Lammertsma AA, et al. Comparison of methods for analysis of clinical [11C]raclopride studies. J Cereb Blood Flow Metab. 1996; 16(1):42–52. [PubMed: 8530554]
23. Slifstein M, et al. Striatal and extrastriatal dopamine release measured with PET and [(18)F] fallypride. Synapse. 2010; 64(5):350–62. [PubMed: 20029833]
24. Chang L, et al. Decreased brain dopamine transporters are related to cognitive deficits in HIV patients with or without cocaine abuse. Neuroimage. 2008; 42(2):869–78. [PubMed: 18579413]
25. Vigorito M, LaShomb AL, Chang SL. Spatial learning and memory in HIV-1 transgenic rats. J Neuroimmune Pharmacol. 2007; 2(4):319–28. [PubMed: 18040850]
26. Torres-Munoz J, et al. Detection of HIV-1 gene sequences in hippocampal neurons isolated from postmortem AIDS brains by laser capture microdissection. J Neuropathol Exp Neurol. 2001; 60(9):885–92. [PubMed: 11556545]
27. Torres-Munoz JE, Nunez M, Petito CK. Successful application of hyperbranched multidisplacement genomic amplification to detect HIV-1 sequences in single neurons removed from autopsy brain sections by laser capture microdissection. J Mol Diagn. 2008; 10(4):317–24. [PubMed: 18556769]
28. Kovalevich J, Langford D. Neuronal toxicity in HIV CNS disease. Future Virol. 2012; 7(7):687–698. [PubMed: 23616788]
29. Mocchetti I, Bachis A, Avdoshina V. Neurotoxicity of Human Immunodeficiency Virus-1: Viral Proteins and Axonal Transport. Neurotox Res. 2011
30. Guha D, et al. Neuronal apoptosis by HIV-1 Vpr: contribution of proinflammatory molecular networks from infected target cells. J Neuroinflammation. 2012; 9:138. [PubMed: 22727020]
31. Rao JS, et al. Increased neuroinflammatory and arachidonic acid cascade markers, and reduced synaptic proteins, in brain of HIV-1 transgenic rats. J Neuroinflammation. 2011; 8(1):101. [PubMed: 21846384]
32. Agrawal L, et al. HIV-1 Tat neurotoxicity: a model of acute and chronic exposure, and neuroprotection by gene delivery of antioxidant enzymes. Neurobiol Dis. 2012; 45(2):657–70. [PubMed: 22036626]
33. Hu S, et al. Preferential sensitivity of human dopaminergic neurons to gp120-induced oxidative damage. J Neurovirol. 2009; 15(5–6):401–10. [PubMed: 20175694]
34. Bezzi P, et al. CXCR4-activated astrocyte glutamate release via TNFalpha: amplification by microglia triggers neurotoxicity. Nat Neurosci. 2001; 4(7):702–10. [PubMed: 11426226]
35. Radja F, et al. Oligodendrocyte-specific expression of human immunodeficiency virus type 1 Nef in transgenic mice leads to vacuolar myelopathy and alters oligodendrocyte phenotype in vitro. J Virol. 2003; 77(21):11745–53. [PubMed: 14557659]

36. Nath A, et al. Synergistic neurotoxicity by human immunodeficiency virus proteins Tat and gp120: protection by memantine. Annals of neurology. 2000; 47(2):186–94. [PubMed: 10665489]
37. Keswani SC, et al. Schwann cell chemokine receptors mediate HIV-1 gp120 toxicity to sensory neurons. Annals of neurology. 2003; 54(3):287–96. [PubMed: 12953261]
38. Hudson L, et al. Detection of the human immunodeficiency virus regulatory protein tat in CNS tissues. Journal of neurovirology. 2000; 6(2):145–55. [PubMed: 10822328]
39. Yeung MC, Pulliam L, Lau AS. The HIV envelope protein gp120 is toxic to human brain-cell cultures through the induction of interleukin-6 and tumor necrosis factor-alpha. AIDS. 1995; 9(2): 137–43. [PubMed: 7536422]
40. Ferris MJ, et al. In vivo microdialysis in awake, freely moving rats demonstrates HIV-1 Tat-induced alterations in dopamine transmission. Synapse. 2009; 63(3):181–5. [PubMed: 19086089]
41. Kessler RM, et al. Occupancy of striatal and extrastriatal dopamine D2 receptors by clozapine and quetiapine. Neuropsychopharmacology : official publication of the American College of Neuropsychopharmacology. 2006; 31(9):1991–2001. [PubMed: 16738543]
42. Riccardi P, et al. Amphetamine-induced displacement of [18F] fallypride in striatum and extrastriatal regions in humans. Neuropsychopharmacology : official publication of the American College of Neuropsychopharmacology. 2006; 31(5):1016–26. [PubMed: 16237395]
43. Narendran R, et al. Positron emission tomography imaging of amphetamine-induced dopamine release in the human cortex: a comparative evaluation of the high affinity dopamine D2/3 radiotracers [11C]FLB 457 and [11C]fallypride. Synapse. 2009; 63(6):447–61. [PubMed: 19217025]
44. Tantawy MN, et al. [(18)F]Fallypride dopamine D2 receptor studies using delayed microPET scans and a modified Logan plot. Nuclear medicine and biology. 2009; 36(8):931–40. [PubMed: 19875049]
45. Honer M, et al. Dynamic imaging of striatal D2 receptors in mice using quad-HIDAC PET. Journal of nuclear medicine : official publication, Society of Nuclear Medicine. 2004; 45(3):464–70.
46. Martic-Kehl MI, et al. Impact of inherent variability and experimental parameters on the reliability of small animal PET data. EJNMMI research. 2012; 2(1):26. [PubMed: 22682020]
47. Mukherjee J, et al. Brain imaging of 18F-fallypride in normal volunteers: blood analysis, distribution, test-retest studies, and preliminary assessment of sensitivity to aging effects on dopamine D-2/D-3 receptors. Synapse. 2002; 46(3):170–88. [PubMed: 12325044]
48. Dunn JT, et al. Establishing test-retest reliability of an adapted [(18)F]fallypride imaging protocol in older people. Journal of cerebral blood flow and metabolism : official journal of the International Society of Cerebral Blood Flow and Metabolism. 2013; 33(7):1098–103.
49. Mukherjee J, et al. In vitro and in vivo evaluation of the binding of the dopamine D2 receptor agonist (11)C-(R,S)-5-hydroxy-2-(di-n-propylamino)tetralin in rodents and nonhuman primate. Synapse. 2000; 37(1):64–70. [PubMed: 10842352]
50. Tantawy MN, et al. Impact of isoflurane anesthesia on D2 receptor occupancy by [18F]fallypride measured by microPET with a modified Logan plot. Synapse. 2011; 65(11):1173–80. [PubMed: 21584868]

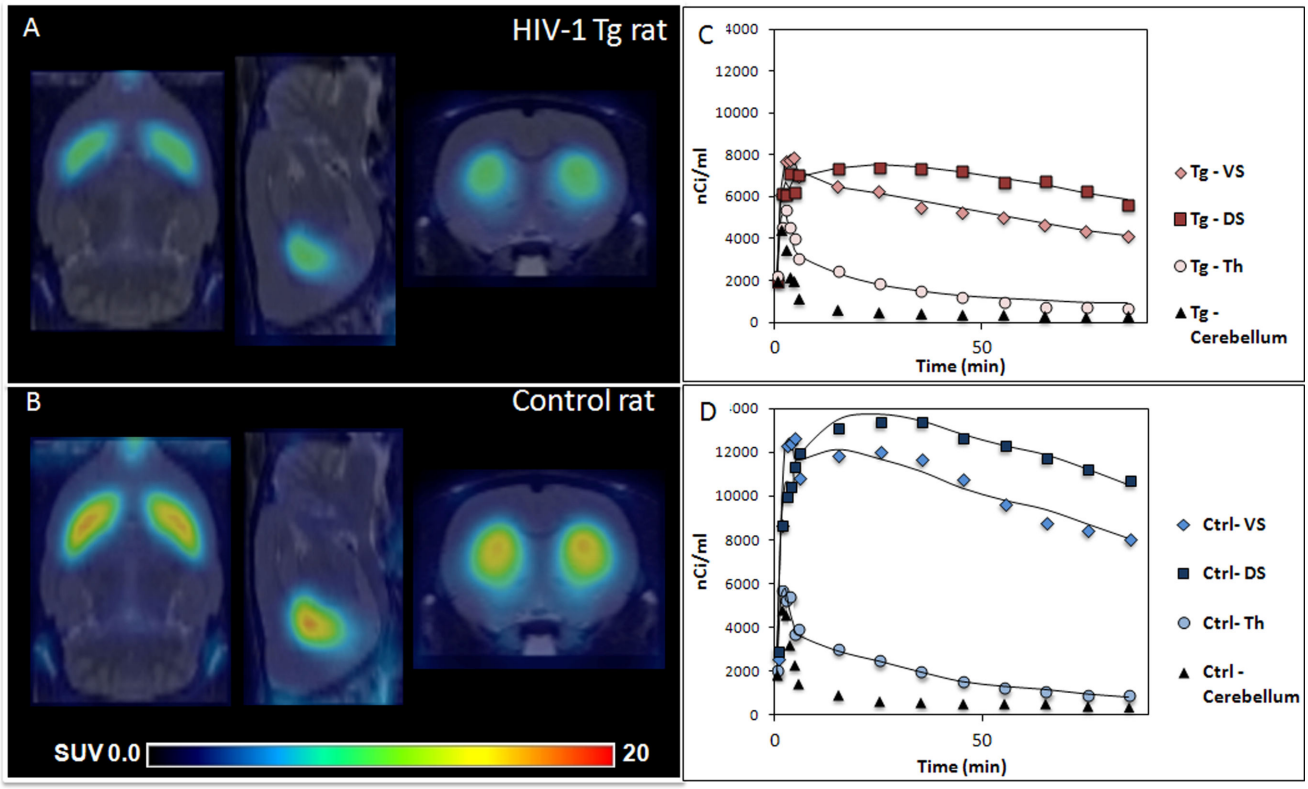

Figure. 1.

Reduced uptake of [^{18}F]fallypride is qualitatively detectable in the Tg rat compared to the control rat. Shown are axial, sagittal, and coronal MR co-registered, normalized [^{18}F]fallypride PET images at the level of the striatum from (A), a representative adult HIV-1 Tg rat and (B), a representative age-matched control. Both images represent summed data from PET acquired between 50 to 90 min after injection and are displayed on a common scale (0–20 SUV, radioactivity normalized by injected dose). Time-activity curves of [^{18}F]fallypride injections obtained from the dorsal striatum (DS) and ventral striatum (VS) (left and right averaged), thalamus (Th), and cerebellum are shown in (C) an adult HIV-1 Tg and (D) an adult control rat. The solid lines represent the quality of data fit obtained using the 2-Tissue reference model with the cerebellum as reference.

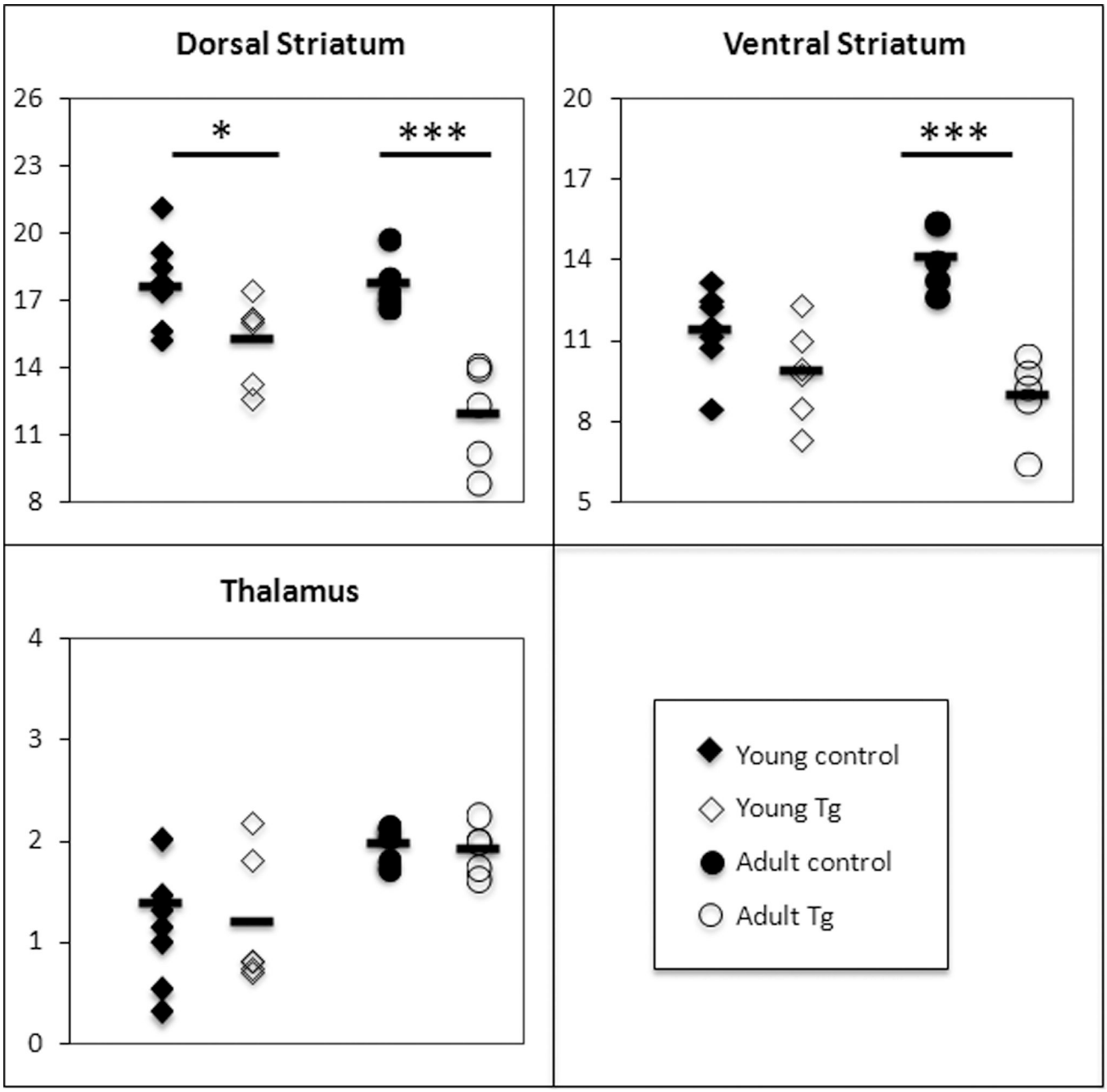

Figure. 2.

Scatter plot of individual BP_{ND} estimates with the selective $D_{2/3}$ antagonist [^{18}F]fallypride and PET in young (n=6) and adult (n=5) HIV-1 Tg rats and young (n=7) and adult (n=5) control rats. The mean BP_{ND} for each region and group is indicated by a small horizontal line. The estimates of BP_{ND} in the young HIV-1 Tg rats were significantly reduced in the dorsal striatum (14%; *p<0.05) with a trend reduction in the ventral striatum (14%; p=0.11). In the older HIV-1 Tg rats, decreases were significant in the dorsal (33%; ***p<0.001) and ventral (36%; ***p<0.001) striatal ROIs compared to controls. No significant BP_{ND} reduction was observed in the thalamus of the Tg rats compared to controls, neither in the young nor in the adult groups.

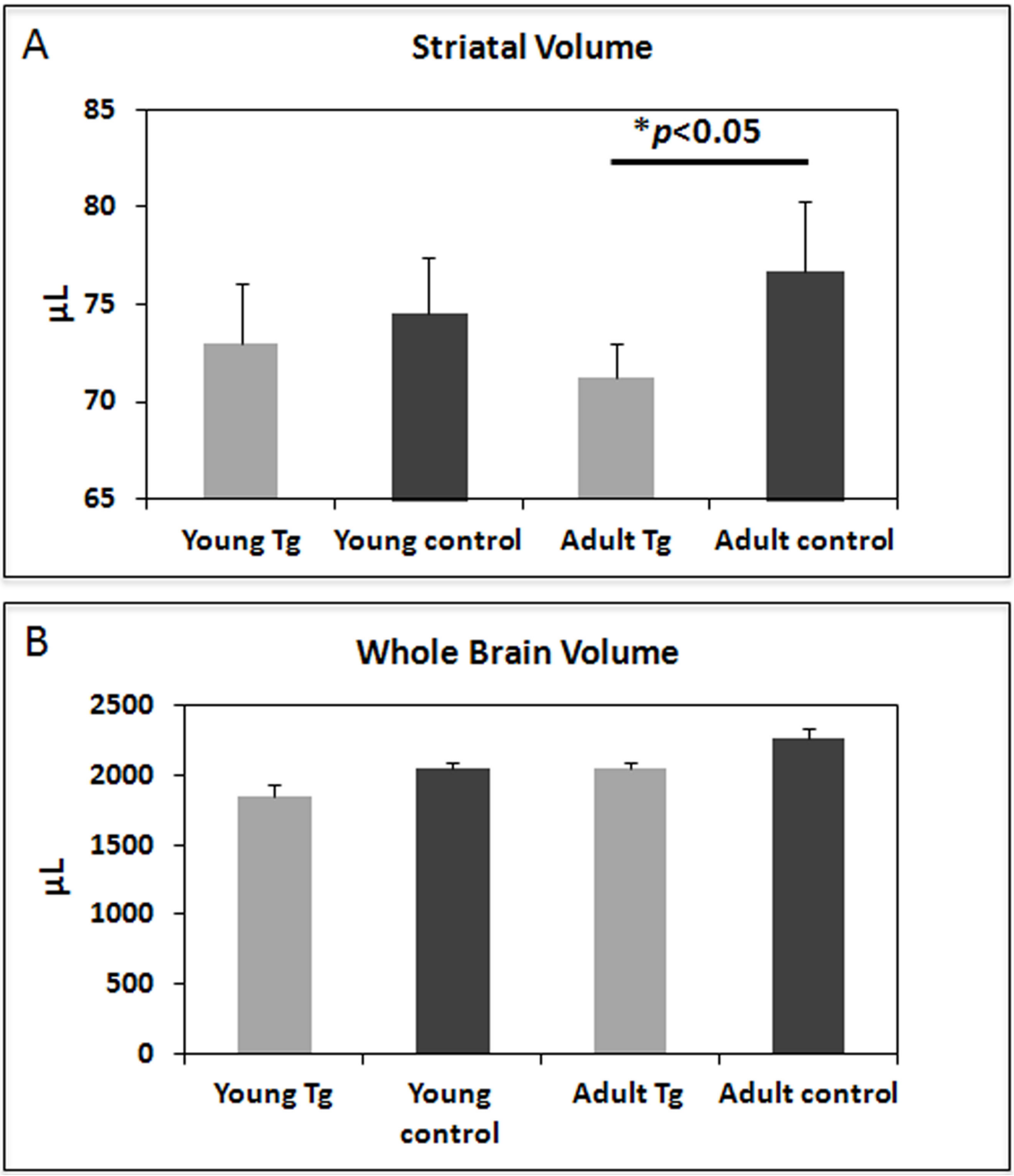

Figure. 3.

Volumetric MR measurements of representative sections of the striatum (A) and of the whole brain (B) in young and adult HIV-1 Tg rats compared to controls. Striatal volumes were reduced (8%; $p<0.05$) in the adult but not in the young Tg rats when compared to their respective age-matched controls. A pattern of accelerated striatal volume loss in the adult Tg rats, out of proportion to the degree of whole brain volume loss, is not seen in control rats.

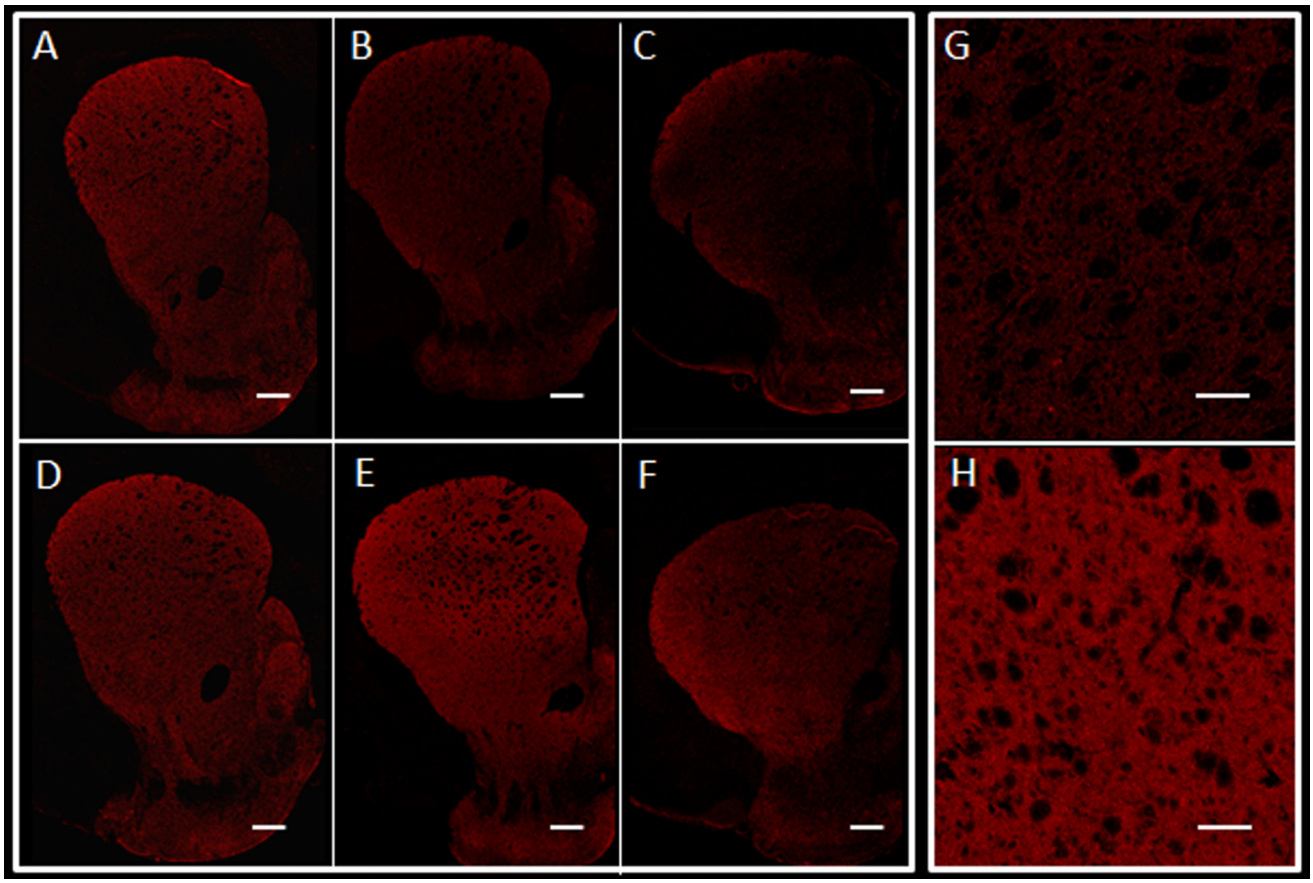

Figure. 4.

Immunohistochemistry (immunofluorescence): striatal sections (3×) stained for TH (red), obtained from a 3 month-old Tg (A), 7 month-old Tg (B) and 17-month-old Tg (C) rats and corresponding age-matched control rats (D, E and F). Decreased TH staining is seen in the Tg animals but is least noticeable in the youngest rats. The pattern of involvement appears diffuse in panel B, while in panel C it appears more focal, with greatest decreased staining seen medially (magnification: 3×, scale bar 500 μm). Panels G and H show higher magnification images from the 7-month old Tg and control animals shown in B and E. Decreased TH staining is again appreciated in the Tg compared to the control animal (magnification: 25×, scale bar 100μm).